ChemComm

COMMUNICATION

View Article Online
View Journal

Cite this: DOI: 10.1039/d5cc04421a

Received 2nd August 2025,
Accepted 9th September 2025

DOI: 10.1039/d5cc04421a

rsc.li/chemcomm

Reconciling color purity and redox potential in electrochromic materials *via* electronic-state-informed molecular design

Daisuke Goto[ab] and Hirotoshi Mori *[a]

Reconciling vivid coloration and low oxidation potential in electrochromic materials—essential for functional devices such as displays, sensors, and energy systems—remains a key challenge due to intrinsic electronic trade-offs. Here we establish a generalizable design strategy based on electronic-state informatics, integrating quantum chemical calculations with machine learning, to identify and experimentally validate a triphenylamine-based compound that exhibits pure yellow color (h = 93.6°) and low oxidation potential (E_{ox} = 0.12 V). While demonstrated here for electrochromic materials, our interpretable, data-driven framework is broadly applicable to the multi-objective design of π-conjugated molecules, including emitters, absorbers, and charge-transporting materials. This approach moves beyond empirical trial-and-error, offering a rational and generalizable methodology for property-driven molecular engineering.

Functional molecular materials that undergo tunable redox-driven transformations are essential for next-generation optoelectronic devices. Among them, organic electrochromic (OEC) materials have attracted considerable attention due to their low energy consumption, high color contrast, and compatibility with flexible substrates.[1–3] While significant progress has been made in expanding the color gamut and improving device durability,[4–12] a central design challenge remains: the simultaneous optimization of color purity and device-compatible oxidation potential (E_{ox})—two properties that are often electronically at odds.[13] Here, color purity is the color deviation in CIE space,[14] and device-compatibility refers to a low oxidation potential for stability and low power consumption.

This trade-off is particularly severe in the case of yellow electrochromism, which requires the radical state to absorb in the long-wavelength visible region (λ = 570–600 nm) without destabilizing the material through excessively low oxidation potentials (E_{ox}) that exceed practical thresholds. As a result, no single molecular scaffold has yet enabled the simultaneous realization of all three subtractive primaries—cyan, magenta, and yellow (CMY)—with both high color purity in their respective radical states and electrochemically stable low E_{ox} values.

Triphenylamine (TPA) has emerged as a versatile redox-active scaffold for OEC applications. Its moderately flexible, nitrogen-centered three-dimensional geometry supports a wide HOMO–LUMO gap and optical transparency in the reduced state. Upon oxidation, TPA derivatives exhibit SOMO-induced color transitions, which can be precisely tuned through substituent and bridging modifications on the aryl rings,[15–17] as guided by electronic state informatics[18–21] (see Fig. 1). However, although high color purity had been achieved in previous studies, the oxidation potential had not been simultaneously optimized for device compatibility. In this study, we report an advancement by demonstrating that pure yellow coloration and a device-compatible E_{ox} can be simultaneously realized in a TPA-based electrochromic material, thereby completing the CMY color palette both optically and electrochemically.

We developed a six-stage design and screening workflow to achieve the simultaneous optimization of coloration and electrochemical stability required for practical OEC devices (Fig. 2). This approach integrates large-scale chemical space exploration, semiempirical electronic structure calculations, and

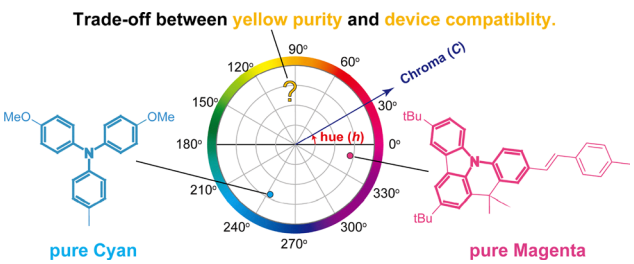

Fig. 1 Target of this study: OEC materials with a single scaffold.

[a] Department of Applied Chemistry, Faculty of Science and Engineering, Chuo University, 1-13-27 Kasuga, Bunkyo-ku, Tokyo, Japan. E-mail: qc-forest.19d@g.chuo-u.ac.jp; Tel: +81 338171918
[b] Advanced Technology Research and Development Division, Ricoh, Company, Limited, Ebina, Kanagawa 243-0460, Japan

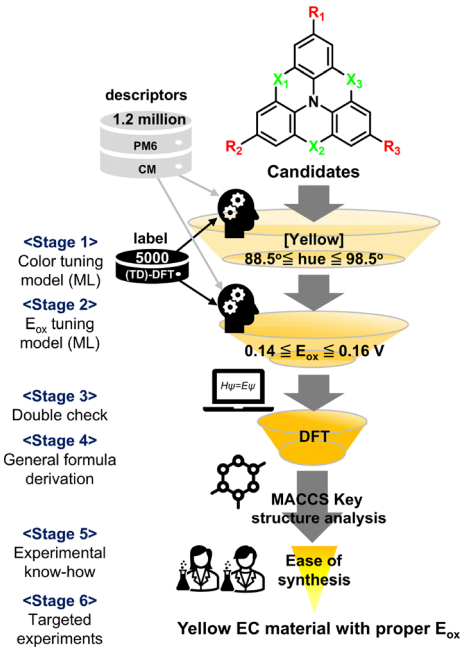

Fig. 2 Screening scheme.

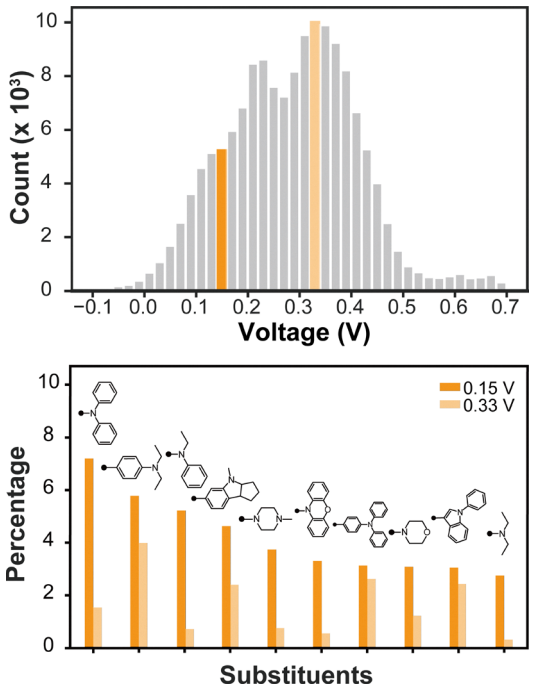

Fig. 3 (top) Predicted E_{ox} distribution. (bottom) Substituents' statistics at E_{ox} = 0.15/0.33 V (5231/10 052 compounds).

machine learning (ML) predictions to optimize both coloration and E_{ox} in a data-driven manner.[17]

Specifically, we constructed a virtual molecular library of over 1.2 million TPA derivatives by combining 11 crosslinking groups (X_1–X_3; Table S1) with 53 π-substituent groups (R_1–R_3; Table S2). Initial molecular structures were generated from SMILES using Open Babel,[22] labels consisted of hue angles (h) and E_{ox} obtained at the TD-CAM-B3LYP/6-31G(d) level, with all structures confirmed to be energy minima by frequency analysis.

For descriptors, we adopted frontier orbital energies calculated at the PM6[23] level and eigenvalues of the Coulomb matrix[24] (CM) to represent the electronic and structural characteristics of candidate molecules (Fig. S3 and S4). Based on these, we constructed ML models including linear regression (LR), support vector regression (SVR), and gradient boosting decision trees (GBDT) to predict molecules that would exhibit pure yellow coloration (h = 93.5°) upon oxidation with E_{ox} of approximately 0.15 V (*vs.* Fc/Fc^+). For E_{ox} prediction, we achieved a coefficient of determination R^2 = 0.88 (Fig. S5–S7 and Table S5).

The narrowed-down molecular candidates were reevaluated using TDDFT at stage 3, and design principles were extracted through MACCS key structure analysis at stage 4. Based on the obtained insights, structurally simple TPA-based chromophores were synthesized and evaluated at stage 5 (SI, Sections S2 and S3). Finally, spectroelectrochemical measurements were performed to demonstrate the OEC properties at stage 6.

Among the LR, SVR, and GBDT, GBDT performed the best for the color prediction, with CMAE = 30° (conditional mean absolute error; Fig. S6). In the oxidized states, 150 000 candidate molecules were predicted to exhibit yellow (88.5° ≤ h ≤ 98.5°).

Introducing radical cation features, we could also obtain the E_{ox} model with enough chemical accuracy (R^2 = 0.88, Fig. S7, S8 and Table S4). The model predicted a wide distribution of E_{ox} from −0.05 to +0.7 V (Fig. 3, top). The broadness implies that appropriate bridging and substituents introduction must be required to control the E_{ox} of yellow OEC materials to be 0.15 V. These results underscore the complexity of molecular design in achieving specific electrochemical properties while maintaining the desired optical characteristics. Focusing on the optimal E_{ox} range (0.14 ≤ E_{ox} ≤ 0.16 V), the number of candidates was further narrowed to 5231.

The substituents' statistics of the candidate molecules indicate that nitrogen-containing substituents would give the desired oxidation potential (E_{ox} = 0.15 V) for the yellow OEC material (Fig. 3, bottom). After double-checking for the yellow coloration and E_{ox} of the molecules with TD-CAM-B3LYP/6-31G(d) calculation, the number of candidates was reduced to 887.

To ensure the structural motifs identified in this narrowed set of 5231 candidates were statistically significant—and not simply a result of sampling from the much larger population of 150 000 yellow candidates—we performed a rigorous statistical comparison. Specifically, by comparing molecules with optimal potential against those arbitrarily sampled using Fisher's exact test of MACCS keys (Table S6), we obtained a clear and robust guideline for molecular design that exhibits yellow coloration with optimal E_{ox} (Fig. 4).

Introducing a phenyl/biphenyl group sandwiched between two nitrogen atoms without introducing any cross-linking group would reproduce yellow coloration upon oxidation near E_{ox} = 0.15 V. Along the guideline, 25 non-crosslinked molecules

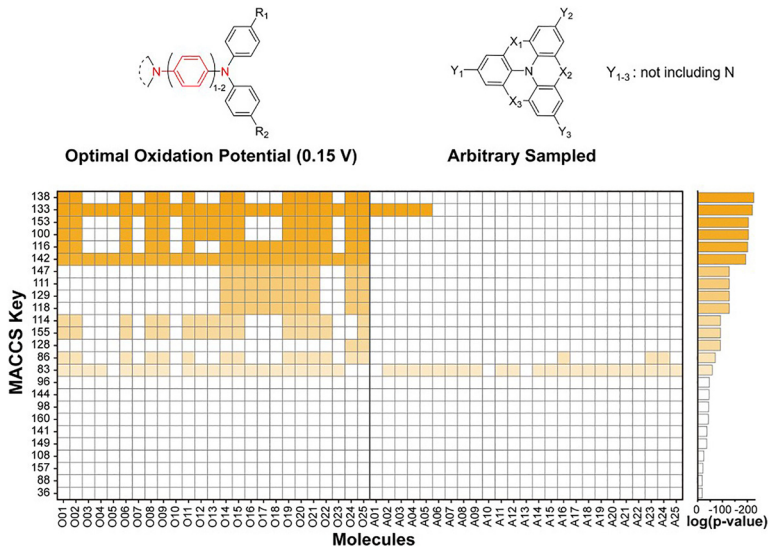

Fig. 4 MACCS key analysis (Table S4) for the candidates with optimal oxidation potential and arbitrary sampled (O01-25 and A01-25; Chart S1). The *p*-substituent (R_1–R_2) and cross-linking (X_1–X_3) groups are defined in Tables S1 and S2.

that are easy to synthesize were selected, and their h and E_{ox} were evaluated using TD-DFT (Chart S1 and Table S7).

Investigating known OEC materials satisfying the above molecular design guideline, two compounds of particular interest, **PDA** and **DDATA**, were identified.[25,26] However, it had been experimentally reported that both **PDA** and **DDATA** do not exhibit pure yellow but do a greenish-yellow coloration in their oxidized states (Fig. 5).

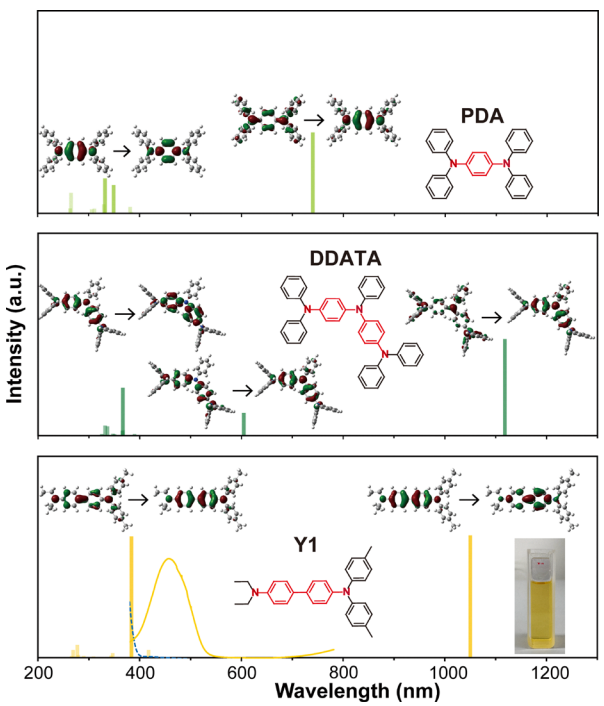

Fig. 5 NTO (TD-CAM-B3LYP/6-31G(d)) for the oxidized **PDA**, **DDATA**, and **Y1**. Experimental data of **Y1** for the oxidized/reduced **Y1** are also depicted with solid/dashed lines.

Using natural transition orbital (NTO) analysis,[27] we clarified that the undesired coloration originated from a set of intervalence charge transfer (IVCT) bands tailing the visible region. In pursuit of our goal to create pure yellow OEC materials with optimal E_{ox}, we focused on molecules incorporating *N*,*N*-diethylaniline—the second most frequent motif among optimal hits, which had not been studied previously. To enhance electrochemical stability,[28] methyl substitutions at the R_2 and R_3 positions were introduced (**Y1**). TDDFT calculation for **Y1** did not predict any IVCT-derived absorption in the visible region in the oxidized state. The IVCT band for **Y1** was at 1050 nm due to a longer N–N distance than **PDA** and **DDATA**. These results suggest that **Y1** would have more potential to function as yellow OEC materials with excellent contrast (Fig. 5).

Finally, the target synthesis of the candidate compound **Y1** was performed in a single step using the Suzuki–Miyaura coupling from commercially available reagents. The yield was over 80% (SI, Section S2 and Fig. S9–S12). Spectroelectrochemical experiments corroborated the TDDFT calculations, showing that **Y1** is completely transparent in its reduced state (Fig. 5 and Fig. S13). Upon oxidation, IVCT band of **Y1** does not extend into the visible region (1180 nm), resulting in a pure yellow (h = 93.6°; Table 1, Fig. 5 and Fig. S14). Cyclic voltammetry and differential pulse voltammetry revealed that **Y1** has an E_{ox} of 0.12 V (*vs.* Fc/Fc^+), confirming its suitability for device operation (Fig. S15 and S16). Compared to previously known OEC materials, the approach combining electronic structure informatics with subsequent organic synthesis and spectroelectrochemistry experiments has successfully realized an OEC material that meets all required conditions for practical OEC devices (Table 1).

The novelty of **Y1** lies in its balanced optoelectronic performance, simultaneously achieving a pure yellow hue and device-compatible E_{ox}. This co-optimization, realized through informed

Table 1 Comparison of electrochemical and optical properties

Material	E_{ox}[a]/V	h/deg.	Ref.
Y1	0.12	93.6 (92.9)	This study
ACE3	0.347	95.9	Christiansen *et al.*[29]
M5	0.15	108.0[b]	Wang *et al.*[30]

[a] Converted by $E_{ox}(Fc/Fc^{+}) = E_{ox}(Ag/AgCl) - 0.44$ V. [b] Chemical oxidation data.

motif selection and rigorous statistical and electronic-state analyses, overcomes the trade-offs that have hindered previous systems and is validated by both theoretical and experimental evidence.

In summary, we reconcile the intrinsic trade-off between color purity and low oxidation potential in organic electrochromic materials using electronic-state informatics. By integrating semi-empirical/DFT quantum chemical calculations with machine learning and statistical validation, we uncovered an interpretable design rule—favoring nitrogen-centered substituents and non-crosslinked frameworks—that enables the simultaneous optimization of competing optical and redox properties. This rule guided the successful synthesis and spectroelectrochemical validation of a pure yellow molecule with ultra-low E_{ox} (0.12 V), underscoring the practical utility of the method.

Beyond the scope of electrochromics, the proposed strategy establishes a general framework for multi-objective molecular design applicable to a wide range of organic electronics. Its interpretable nature and statistical rigor offer an advancement over conventional trial-and-error or heuristic approaches, contributing to a more rational and transferable molecular design paradigm across materials science.

Conflicts of interest

There is no conflict to declare.

Data availability

Supporting data are provided in the SI. Machine learning and experimental details (PDF), Library geration program (ZIP). See DOI: **https://doi.org/10.1039/d5cc04421a**.

Due to its size, the full theoretical database is not included, but the PM6 optimized structures, predicted energies, and associated code are available from the authors upon reasonable request.

The calculations were performed using resources provided by the Research Center for Computational Science (RCCS) at the Okazaki Research Facilities of the National Institutes of Natural Sciences (NINS), Japan (Project no. 25-IMS-C014).

Notes and references

1 Y. Zhai, J. Li, S. Shen, Z. Zhu, S. Mao, X. Xiao, C. Zhu, J. Tang, X. Lu and J. Chen, *Adv. Funct. Mater.*, 2022, **32**, 2109848.
2 A. L.-S. Eh, A. W. M. Tan, X. Cheng, S. Magdassi and P. S. Lee, *Energy Technol.*, 2018, **6**, 33–45.
3 H. Liang, R. Li, C. Li, C. Hou, Y. Li, Q. Zhang and H. Wang, *Mater. Horiz.*, 2019, **6**, 571–579.
4 M. N. Mustafa, M. A. A. Mohd Abdah, A. Numan, A. Moreno-Rangel, A. Radwan and M. Khalid, *Renewable Sustainable Energy Rev.*, 2023, **181**, 113355.
5 S. Wu, H. Sun, M. Duan, H. Mao, Y. Wu, H. Zhao and B. Lin, *Cell Rep. Phys. Sci.*, 2023, **4**, 101370.
6 G. A. Niklasson and C. G. Granqvist, *J. Mater. Chem.*, 2007, **17**, 127–156.
7 R. Tallberg, B. P. Jelle, R. Loonen, T. Gao and M. Hamdy, *Sol. Energy Mater. Sol. Cells*, 2019, **200**, 109828.
8 A. Cannavale, U. Ayr, F. Fiorito and F. Martellotta, *Energies*, 2020, **13**, 1449.
9 J. Kim, M. Rmond, D. Kim, H. Jang and E. Kim, *Adv. Mater. Technol.*, 2020, **5**, 1900890.
10 C. G. Granqvist, l Bayrak Pehlivan and G. A. Niklasson, *Surf. Coat. Technol.*, 2018, **336**, 133–138.
11 S. Zhao, B. Wang, N. Zhu, Y. Huang, F. Wang, R. Li, Y. Zhao, Q. Jiang, X. Wu and R. Zhang, *Carbon Neutralization*, 2023, **2**, 4–27.
12 R. Baetens, B. P. Jelle and A. Gustavsen, *Sol. Energy Mater. Sol. Cells*, 2010, **94**, 87–105.
13 C. G. Tang, K. Hou and W. L. Leong, *Chem. Mater.*, 2024, **36**, 28–53.
14 K. Mclaren, *J. Soc. Dyers Colour.*, 1976, **92**, 338–341.
15 A. Mizuno, R. Matsuoka, T. Mibu and T. Kusamoto, *Chem. Rev.*, 2024, **124**, 1034–1121.
16 D. Goto and H. Mori, *J. Phys. Chem. Lett.*, 2024, **15**, 8205–8210.
17 D. Goto, Y. Kanebako, K. Takashima, N. Kuroki and H. Mori, *J. Phys. Chem. Lett.*, 2025, **16**, 2419–2424.
18 R. Suzuki and H. Mori, *J. Phys. Chem. A*, 2025, **129**, 2612–2617.
19 N. Kuroki, D. Kodama, Y. Suzuki, F. Chowdhury, H. Yamada and H. Mori, *J. Phys. Chem. B*, 2023, **127**, 2022–2027.
20 S. Watabe, N. Kuroki and H. Mori, *ACS Omega*, 2023, **8**, 14478–14483.
21 F. Weber and H. Mori, *Npj Comput. Mater.*, 2022, **8**, 176.
22 N. M. O'Boyle, M. Banck, C. A. James, C. Morley, T. Vandermeersch and G. R. Hutchison, *J. Cheminform.*, 2011, **3**, 1–14.
23 J. J. P. Stewart, *J. Mol. Model.*, 2007, **13**, 1173–1213.
24 M. Rupp, A. Tkatchenko, K.-R. Müller and O. A. von Lilienfeld, *Phys. Rev. Lett.*, 2012, **108**, 058301.
25 Z. Lin, J. Ye, S. Shinohara, Y. Tanaka, R. Yoshioka, C.-Y. Chan, Y.-T. Lee, X. Tang, K. Mitrofanov and K. Wang, *et al.*, *Nat. Commun.*, 2025, **16**, 2686.
26 Y.-C. Chung and Y. O. Su, *J. Chin. Chem. Soc.*, 2009, **56**, 493–503.
27 R. L. Martin, *J. Chem. Phys.*, 2003, **118**, 4775–4777.
28 A. Vasievska and T. Slanina, *Chem. Commun.*, 2024, **60**, 252–264.
29 D. T. Christiansen, A. L. Tomlinson and J. R. Reynolds, *J. Am. Chem. Soc.*, 2019, **141**, 3859–3862.
30 Y. Wang, S. Wang, X. Wang, W. Zhang, W. Zheng, Y. M. Zhang and S. X. Zhang, *Nat. Mater.*, 2019, **18**, 1335–1342.

